Eur. Phys. J. Appl. Phys. **97**, 23 (2022)

https://doi.org/10.1051/epjap/2022210294

THE EUROPEAN PHYSICAL JOURNAL APPLIED PHYSICS

Regular Article

Improving photovoltaic performance of P3HT: $IC_{60}BA$ based organic solar cell: N-type doping effect

Meriem Erray[1,*], Aumeur El Amrani[1,2], Mounir Hanine[1], Mohamed El Amraoui[3], and Lahcen Bejjit[2]

[1] ERTTI Laboratory, MCSCO research group, FSTE, Moulay Ismail University of Meknes, 52000, BP. 509 Boutalamine, Errachidia, Morocco
[2] MIN research group, Electrical Engineering Department, ESTM, Moulay Ismail University of Meknes, Meknes, Morocco
[3] LASMAR Laboratory, Faculty of Sciences, Moulay Ismail University of Meknes, 50000, B.P. 11201 Zitoune Meknès, Morocco

Received: 18 December 2021 / Received in final form: 27 February 2022 / Accepted: 3 March 2022

Abstract. In this paper we report a numerical simulation study for P3HT: $IC_{60}BA$ based organic solar cell with Analysis of Microelectronic and Photonic Structures the simulation one dimension software (AMPS-1D). Indeed, the N-type doping concentration (N_D) effect on the organic solar cell performance is done. Moreover, a combination between the P-type doping concentration (N_A) and N-type one (N_D) is investigated. However, due to the relationship between doping and carriers charge mobility, the effect of N_D for different electron mobilities (μ_n) is also studied. We showed a high efficiency of 5.88% that is achieved for particular values of $N_A = 10^{17}\,cm^{-3}$, $N_D = 2 \times 10^{16}\,cm^{-3}$, $\mu_p = 3 \times 10^{-4}\,cm^2\,V^{-1}\,s^{-1}$ and $\mu_n = 7 \times 10^{-4}\,cm^2\,V^{-1}\,s^{-1}$. Thus, we noticed that the P-type doping remains more promising than N-type one for the device performance improvement. Furthermore, the validation of the obtained results by those experimentally reported in literature is realized. In addition, the doping of other BHJ OSC devices consisting of P3HT: $IC_{70}BA$ is studied; an optimum efficiency of about 6.32% is reached.

1 Introduction

In these recent years, the organic solar cells (OSCs), and in particular bulk-heterojunction (BHJ), have drawn considerable attention [1–4] due to their multiple advantages such as: flexibility, low cost, diversity of materials, and lightness [5–12]. Generally, the BHJ based OSCs consist of two types of semiconductor; donor and acceptor [13]. Thus, the most studied organic solar cells are based on P3HT: PCBM where the poly (3-hexylthiophene) (P3HT) is used as donor and the soluble C_{60} derivative, [6,6] −phenyl-C_{61}-butyric acid methyl ester (PCBM) as acceptor. Indeed, it was reported that the efficiency of similar devices based on P3HT:PCBM are in the range of 3.84% to 6.82% [14,15]. For their interesting properties, P3HT was selected as a donor material and IC60BA (indene-C60 bisadduct) as acceptor one [16–18]. This last (i.e. $IC_{60}BA$) was synthesized for the first time in 2009 [19]; due to its high LUMO energy level of −3.74 eV (Fig. 1) it will be more used as acceptor instead of PCBM. Thus, it was reported that the organic solar cells based on P3HT:$IC_{60}BA$ can show a high open circuit voltage of 0.84 eV and a good efficiency compared to those based on P3HT: PCBM [19–23]. However, until now their efficiency remain still very low compared to inorganic ones [12]. Therefore, to improve the efficiency of OSCs, different methods have been investigated like: annealing, optimization of donor: acceptor ratio, synthesizing of new organic semiconductors, device structure modification [24–27], and doping [28–31]. This last can be considered as good means for the performances improvement of the OSCs [32,33]; this affect the carriers charge mobility (i.e. transport mechanism). The doping may be classified into P-type and N one. The P-type doping of organic semiconductors is realized with inorganic dopants like: (bromine, Alkali metal, Alkaline earth metals, organometallic compounds) [34–36], or organic ones such as: orthochloranil, 25 tetracyano-quinodimethane (TCNQ), teterafluoro-tetracyanon (F4-TCNQ) or dicyano-dichloroquinone (DDQ) [29–31,37–39]. In addition, the N-type doping of organic semiconductors was investigated for the first time by using inorganic dopants (halogen, transition metal salts or alkalines: caesium) [36,40]. However, these last years it was reported that the N-type doping with an organic dopant (benzylviologen (BV)) can improve the performances of OSCs [41]. In addition, the doping remains one of the most concepts for organic semiconductor devices design and engineering. However, it requires more understanding because the doping in organic materials differs from those in traditional inorganic ones. Thus, the most organic devices are not often doped; however unintentional doping can always take place during the realization. This means that the doping approach should be investigated for organic semiconductors. Moreover, the different doping methods, ranging from chemical solution to physical diffusion doping are among the major complications for an organic solar cell device structure.

* e-mail: m.erray@edu.umi.ac.ma

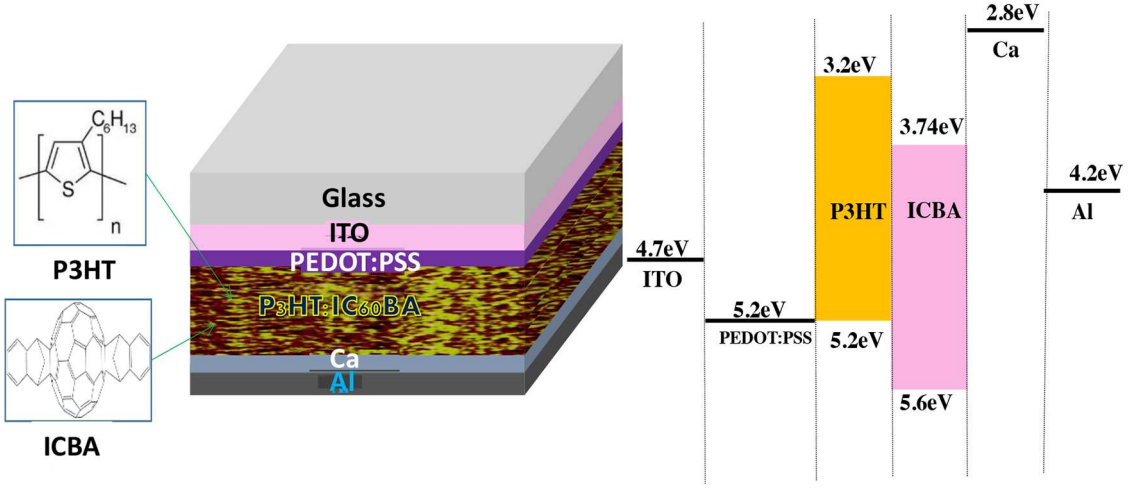

Fig. 1. Organic solar cell based on ITO/PEDOT: PSS/P3HT:$IC_{60}BA$/Ca/Al structure [39].

Thus, because of their instability few published research works concerning the N-type doping have been reported [41]. Moreover, the doping with an organic element can be realized by thermal evaporation [42], co-sublimation [31], electrochemical doping [43], ion implantation doping [36,44] and solution-processing through liquid phase [33,42]. This last method remains the most used by researchers, and it consists of mixing the material to be doped with the desired dopant in liquid phase, then the deposition of the obtained blend solution by using spin coating (Fig. 2).

In this present work, we report a simulation study of the doping effect on the performances of the organic solar cell based on P3HT: $IC_{60}BA$. However, the P-type doping effect on the performances of this similar structure has been already investigated with AMPS-1D software by Erray et al. [39]. Therefore, in this present research work, the N-type doping effect is done, which is considered as an original approach associated to that reported in our previously work [39]. Moreover, a combination between the effects of doping concentration and the electrons mobility has been investigated. Thus, the optimization of doping concentrations N_A and N_D for P3HT: $IC_{60}BA$ device has been realized. In addition, the validation of the obtained results by those experimentally reported in literature has been reported. Finally, the doping was investigated for another structure such as P3HT: $IC_{70}BA$ based BHJ OSC.

2 Simulation method

In order to investigate the N-type doping effect on the performances of the OSC based on P3HT: $IC_{60}BA$, several experiment errors can be induced; this will be costly. Therefore, the AMPS-1D (Analysis of Microelectronic and Photonic Structures one dimension) simulator program can be used to simulate the ITO/PEDOT:PSS/P3HT: $IC_{60}BA$/Ca/Al based organic solar cell structure, where its electrical model is based on the Poisson's equation (Eq. (1)), the continuity equations for holes (Eq. (2)) and for electrons (Eq. (3)), and the equations (4) and (5) for drift-diffusion phenomena [45,46]. Moreover, to simulate the active layer that consists of two non-homogeneous materials P3HT as donor and $IC_{60}BA$ as acceptor, an effective medium model (EMM) can be used [47]. This EMM model is characterized by an average of the acceptor and the donor material properties. Indeed, this active layer has a conduction band corresponding to the lowest unoccupied molecular orbital (LUMO) of the $ICB_{60}A$, and a valence band corresponding to the highest occupied molecular orbital (HOMO) of the P3HT. Thus, the effective gap E_g^{eff} of P3HT: $IC_{60}BA$ can be calculated by (Eq. (6)); the value of E_g^{eff} is about 1.46 eV. In addition, as reported in our previous work [39], the electrical and optical used parameters in our simulation for the ITO/PEDOT: PSS/P3HT: ICBA/Ca/Al structure are given in Table 1. In contrast, some used parameters for the P3HT: $IC_{70}BA$ structure have been taken from literature, and the other ones were chosen in order to have the best fit of the simulated J–V curve to the reported experimentally ones [48].

$$div(\vec{grad}\psi) = \frac{q(N_A{}^- - N_D{}^+ + n - p + n_t - p_t)}{\varepsilon} \quad (1)$$

$$\frac{dJ_p}{\mathrm{d}x} = -q(R(x) - G(x)) \quad (2)$$

$$\frac{dJ_n}{\mathrm{d}x} = q(R(x) - G(x)) \quad (3)$$

$$J_p(x) = J_{\mathrm{d}p} + J_{cp} = -kT\mu_p \frac{\mathrm{d}p}{\mathrm{d}x} + q\mu_p pE(x) \quad (4)$$

$$J_n(x) = J_{dn} + J_{cn} = kT\mu_n \frac{\mathrm{d}n}{\mathrm{d}x} + q\mu_n nE(x) \quad (5)$$

$$E_g^{eff} = E_{LUMO}^A - E_{HOMO}^D. \quad (6)$$

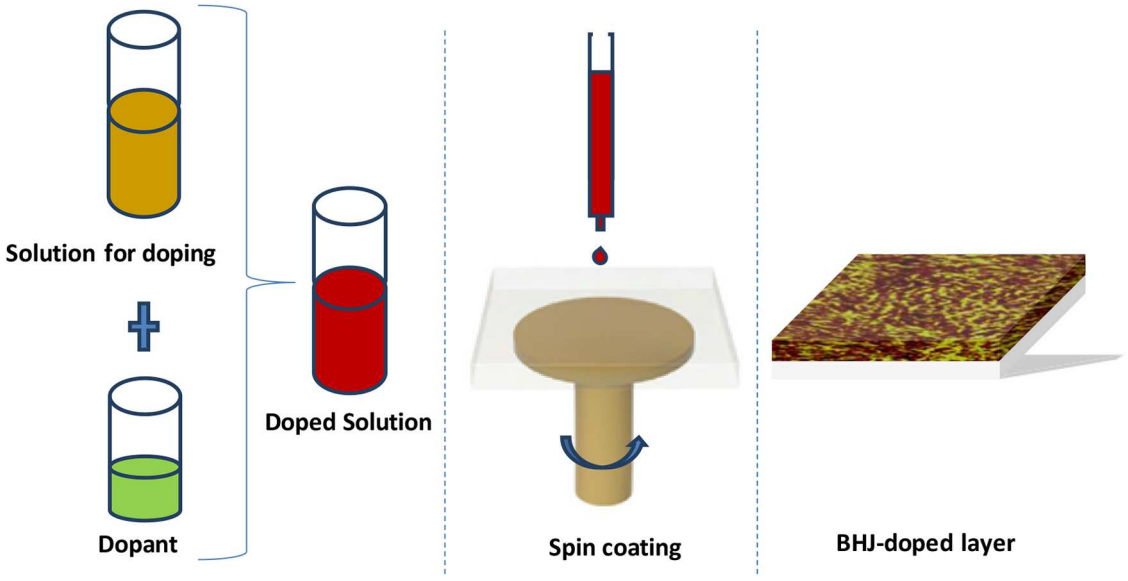

Fig. 2. Chemical method doping: solution-processing through liquid phase.

Table 1. The electrical and optical parameters used in the simulation [39].

Contacts	
Φ_{b0} [eV]	1.3
Φ_{bL} [eV]	0.24
S_{n0}, S_{p0}, S_{nL}, S_{pL} [cm/s]	10^7
R_F	0.1
R_B	0.9
$d_{PEDOT:PSS}$ [nm]	60
Electrical parameters of P3HT: ICBA	
d [nm]	200
ε_r	3.8
μ_n [cm^2/Vs]	Variable
μ_p [cm^2/Vs]	Variable
N_D [cm^{-3}]	Variable
N_A [cm^{-3}]	Variable
E_g^{eff} [eV]	1.46
E_{HOMO}^{A} [eV]	5.67
E_{LUMO}^{A} [eV]	3.74
E_{HOMO}^{D} [eV]	5.2
E_{LUMO}^{D} [eV]	3.2
N_C, N_V [cm^{-3}]	1.5×10^{20}
χ [eV]	3.74
Defects	
G_{D0}, G_{A0} [cm^{-2} eV^{-1}]	3.7×10^{17}
E_D, E_A [eV]	0.04
σ_e, σ_h [cm^2]	1.5×10^{-18}
AM1.5 solar spectrum	Reference [28]

3 Results and discussion

3.1 Effect of N-type and P-type doping concentration on the performances of P3HT: $IC_{60}BA$ based OPV solar cell

As we mentioned above, this present work concerns the *eff*ect of N-type doping on the performances of P3HT: $IC_{60}BA$ based organic solar cell such as: (J_{sc}, V_{oc}, FF and Eff). The simulation studies were realized in the range of 0 cm^{-3} to 1×10^{19} cm^{-3} for different values of P-type doping density: {0 cm^{-3}, 4×10^{16} cm^{-3}, 8×10^{16} cm^{-3}, 1×10^{17} cm^{-3} and 1.2×10^{17} cm^{-3}} by using AMPS-1D. Where, the electrons mobility and holes one are fixed at 7×10^{-4} cm^2 V^{-1} s^{-1} and 3×10^{-4} cm^2 V^{-1} s^{-1}, respectively.

Figure 3 shows the evolution of short-circuit current density (J_{sc}) as function of N-type doping for different values of N_A, where two main behaviors are noticed. On the one hand, a saturation accompanied by low increasing of J_{sc} is showed for N_D less than N_A. We noticed a peak of J_{sc} for the different curves. This peak shifts to a particular value $N_D = N_A$; this shift can be explained by the fact that the active layer returns to its intrinsic state. On the other hand, when N_D increases and $N_D \geq N_A$, a significant fall of J_{sc} is noticed; this reduction in J_{sc} is due to the increase of the concentrations of P-type and N-type dopants. Indeed, the high concentration of dopants leads the defects increase in active layer (P3HT:$IC_{60}BA$), and consequently the reduction of the carrier charges transport *eff*iciency as well as current density J_{sc}.

Figure 4 illustrates the evolution of the open circuit voltage of the investigated device based on P3HT:$IC_{60}BA$ as function of N_D for different values of N_A. We can see that the curves show a similar behavior in particular for N_D in

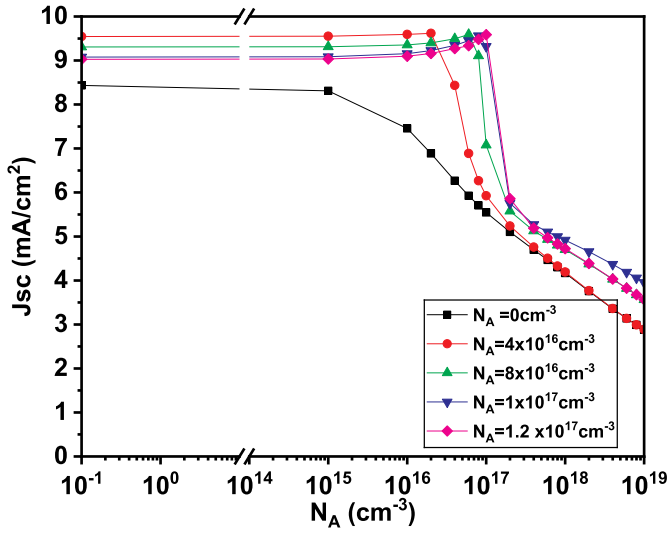

Fig. 3. Variation of the short circuit current density of P3HT: $IC_{60}BA$ based solar cell as function of N_D for different values of N_A.

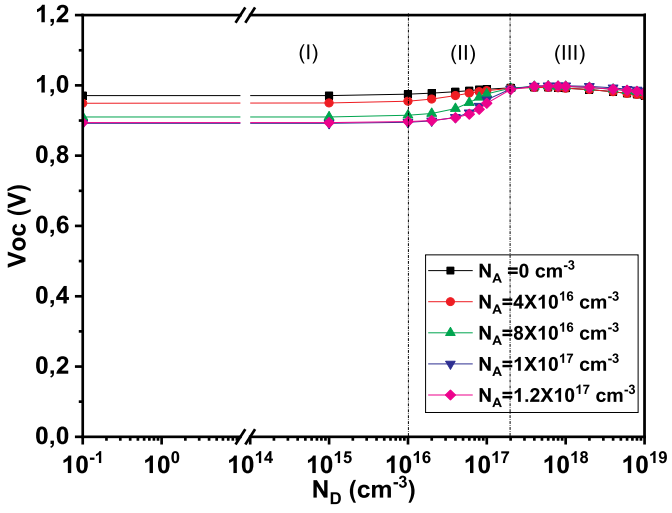

Fig. 4. Evolution of the open circuit voltage for P3HT: $IC_{60}BA$ based solar cell as function of N_D for different values of N_A.

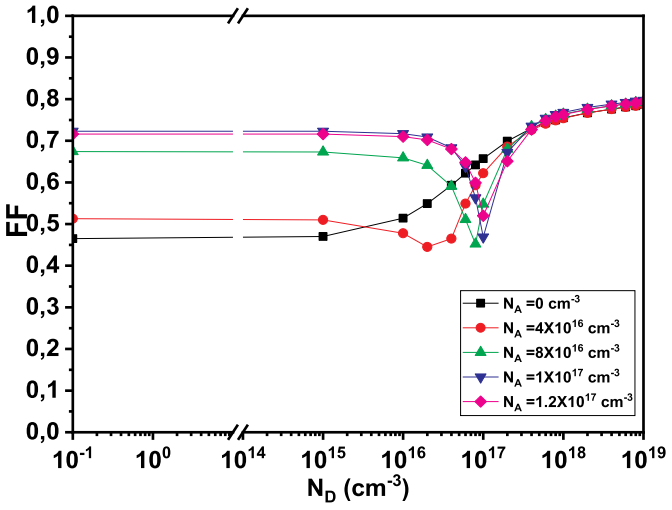

Fig. 5. Variation of the fill factor of P3HT: $IC_{60}BA$ based solar cell as function of N_D for different values of N_A.

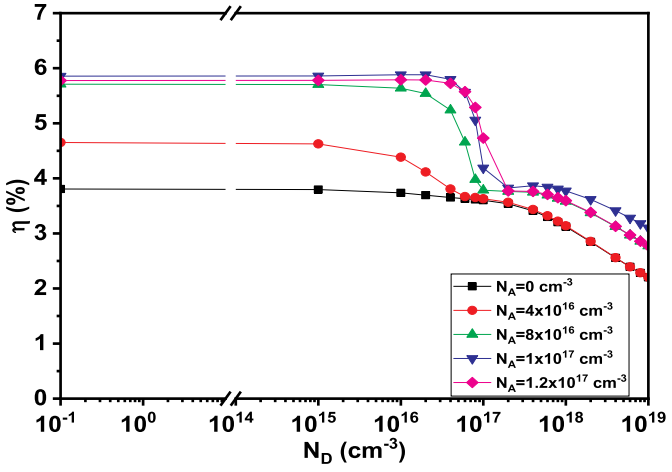

Fig. 6. Evolution of the efficiency of the P3HT: $IC_{60}BA$ based solar cell as function of N_D for different values of N_A.

the range of 0 cm^{-3} to 1×10^{19} cm^{-3}. In addition, three zones are noticed: the first one (I) where N_D varies from 0 cm^{-3} to 1×10^{16} cm^{-3}, where no significant *effect* of N-type doping on the open circuit voltage was showed. However, a relative negative *effect* of P-type doping on V_{oc} was reported, because in this zone N_D remains lower compared to N_A. In the second zone where N_D varied from 1×10^{16} cm^{-3} to 1×10^{17} cm^{-3}, the both N_A and N_D affect the open circuit voltage which it increases relatively with N_D, and on the other hand decreases with N_A. In the last zone (III) where $N_D > 1 \times 10^{17}$ cm^{-3}, the curves are similar for the different values of N_A where also no *effect* on the V_{oc} for the increase of N_D was noticed; as mentioned above, such behavior can be explained by the return of the active layer to its intrinsic state.

Furthermore, Figure 5 presents the evolution of the fill factor (FF) versus N-type doping concentration N_D for different values of N_A. We reported that the FF shows two different behaviors corresponding to the values of P-type doping density (N_A). The first one is noticed for $N_A = 0$ cm^{-3}, where the FF remains practically unchanged with the increase of N_D; this is true only for $N_D < 1 \times 10^{15}$ cm^{-3}. However, over this range the FF increases with N_D. Therefore, we can say that the fact of N-type doping has a beneficial *effect* on the fill factor; which indicates that series resistance decreases with N-type doping concentration. In addition, we showed that these results are in good agreement with that reported in other works [41]. The second behavior concerns the case when N_A is more than 4×10^{16} cm^{-3}, where a saturation of the fill factor is noticed for $N_D < 1 \times 10^{15}$ cm^{-3}, then it starts to decrease with the increase of N_D until $N_D = N_A$, after this, it increases quickly and reaches the saturation.

Figure 6 shows the evolution of the *efficiency* of the P3HT: $IC_{60}BA$ based solar cell versus N_D for different values of N_A. We observed a saturation behavior for the *efficiency* in the range of N_D from 0 cm^{-3} to 1×10^{15} cm^{-3}. However, in this range, a positive *effect* of the P-type

Table 2. Optimal performance of doped OSC based on P3HT: $IC_{60}BA$ with $N_A = 1 \times 10^{17}$ cm^{-3} and $N_D = 2 \times 10^{16}$ cm^{-3}.

Parameters	
η (%)	5.88
FF	0.71
J_{sc} (mA/cm^2)	9.22
V_{oc} (V)	0.92

doping concentration increases on the *efficiency* is noticed; in particular when N_D is less than N_A. In the other hand, we can see a significant reduction of the *efficiency* for N_D between 1×10^{15} cm^{-3} and 1.2×10^{17} cm^{-3}, where a minimum of *efficiency* is achieved at $N_D = N_A$; as we have cited previously, such fall of *efficiency* can be due to the return of the active to its intrinsic state. Moreover, for high density of N_D, the *efficiency* continues to decease; high concentrations of P-type and N-type dopants may lead to create many defects in P3HT: $IC_{60}BA$, which cause the carriers charge transport limitation, and consequently the *efficiency* reduction.

From the above obtained results, and to improve the performances of the investigated device based on P3HT: $IC_{60}BA$, it was shown that the P-type doping is more promising than N-type one. Moreover, the doping with high concentrations of N_D and N_A allows the active layer to return to its electrical intrinsic state with high defects concentration. In addition, the optimum performances of the studied organic solar cell, obtained with AMPS-1D software, were achieved for particular values of $N_A = 1 \times 10^{17}$ cm^{-3} and $N_D = 2 \times 10^{16}$ cm^{-3} (Tab. 2).

3.2 Combined *effects* of N-type doping concentration and electrons mobility

As reported in several research works [33,41,49], the electrons mobility remains more sensitive than holes one with the variation of N-type doping concentration. Therefore, in this present study, the results for the *effect* of N-type doping concentration on the performances of the P3HT: $IC_{60}BA$ solar cell for different values of electrons mobility (μ_n) was illustrated (Fig. 7). The *effect* of N_D was investigated, with AMPS-1D software, in the range of 0 cm^{-3} to 1×10^{19} cm^{-3} for different values of electrons mobility $\mu_n = \{1 \times 10^{-4}$ cm^2 V^{-1} s^{-1}, 3×10^{-4} cm^2 V^{-1} s^{-1}, 7×10^{-4} cm^2 V^{-1} s^{-1}, 3×10^{-3} cm^2 V^{-1} s^{-1} and 3×10^{-2} cm^2 V^{-1} s$^{-1}\}$ and for fixed values of P-type doping concentration ($N_A = 1 \times 10^{17}$ cm^{-3}) and holes mobility ($\mu_p = 3 \times 10^{-4}$ cm^2 V^{-1} s^{-1}).

Figure 7a shows two distinct behaviors concerning the evolution of the short-circuit current density that are governed by the values of electrons mobility. For $\mu_n \leq 3 \times 10^{-4}$ cm^2 V^{-1} s^{-1}, the increase of N_A exhibits a positive *effect* on J_{sc}; a peak is observed at $N_D = 1 \times 10^{17}$ cm^{-3}, which is achieved for a particular value of electrons mobility as well as holes mobility of 3×10^{-4} cm^2 V^{-1} s^{-1}. However, for the electrons mobility $\mu_n \geq 3 \times 10^{-4}$ cm^2 V^{-1} s^{-1}, a similar behavior to that was observed in the case the *effect* of N-type doping concentration for different values of N_A; where a saturation of J_{sc} is noticed in the range of $N_D = 0$ cm^{-3} to $N_D = 1 \times 10^{15}$ cm^{-3}. Over this range, a significant reduction in J_{sc} is noticed.

Furthermore, Figure 7b illustrates the evolution of open circuit voltage of the P3HT: $IC_{60}BA$ based solar cell versus N_D for different values of μ_n. As shown previously in Figure 4, we noticed a similar behavior for V_{oc} evolution with N_D for different values of N_A. However, the highest V_{oc} value corresponds that of electrons mobility $\mu_n = 3 \times 10^{-2}$ cm^2 V^{-1} s^{-1}.

Figure 7c shows the variation of fill factor as function of N_D for different values of μ_n. This figure presents a similar behavior for the different electron mobilities μ_n, where the addition of low quantity of N-type dopants showed indirect *effect* on FF. Indeed, in practice the increase of N_D leads to improve the electrons mobility and consequently causes the enhancement of FF; thus the high value of fill factor was achieved when the ratio μ_n/μ_p is shifted to 1, which remains in good agreement with that reported in other works [33,41]. Thus, for high electrons mobility, the fill factor becomes independent of electrons mobility, but it increases with N_D; this suggests that the series resistance may be also improved [30].

As it was previously observed for the J_{sc}, similar behaviors were noticed concerning the *efficiency* evolution versus N_D for different values of μ_n (Fig. 7d); a peak of *efficiency* is achieved in the case of low electrons mobility and for N_D of about 8×10^{16} cm^{-3}. Thus, the value of this peak is nearly equal to that obtained in the cases of high electrons mobility and low N-type dopant concentration (N_D).

3.3 Application of P-type doping to another similar organic solar cell based on P3HT: $IC_{70}BA$

From the above obtained results and from those reported in reference [39], we can clearly shown that, in order to enhance the performances of an organic solar cell heterojunction, the P-type doping remains more promising than that of N-type doping one. In this present work the P-type doping is investigated also for another organic heterojunction solar cell based on P3HT: $IC_{70}BA$. This device is characterized by a good absorption spectrum compared to P3HT: $IC_{60}BA$, and a higher LUMO energy level (–3.72 eV). Thus, after grouping some electrical and optical parameters from literature while other had been chosen based on the best fit of the simulated J–V curve to the experimental J–V one reported in reference [48], we have found that this device is not in its intrinsic state, however it has been already uncontrollably (i.e. unintentionally) doped with $N_A = 4 \times 10^{16}$ cm^{-3}. Therefore, in order to improve the *efficiency* of this structure, the active layer of the (P3HT: $IC_{70}BA$) based investigated device was also doped with $N_A = 1 \times 10^{17}$ cm^{-3}.

Figure 8 presents J–V characteristics of P3HT: $IC_{70}BA$ based solar cell which are obtained by AMPS-1D software before doping (i.e. unintentionally doping) (blue color) and

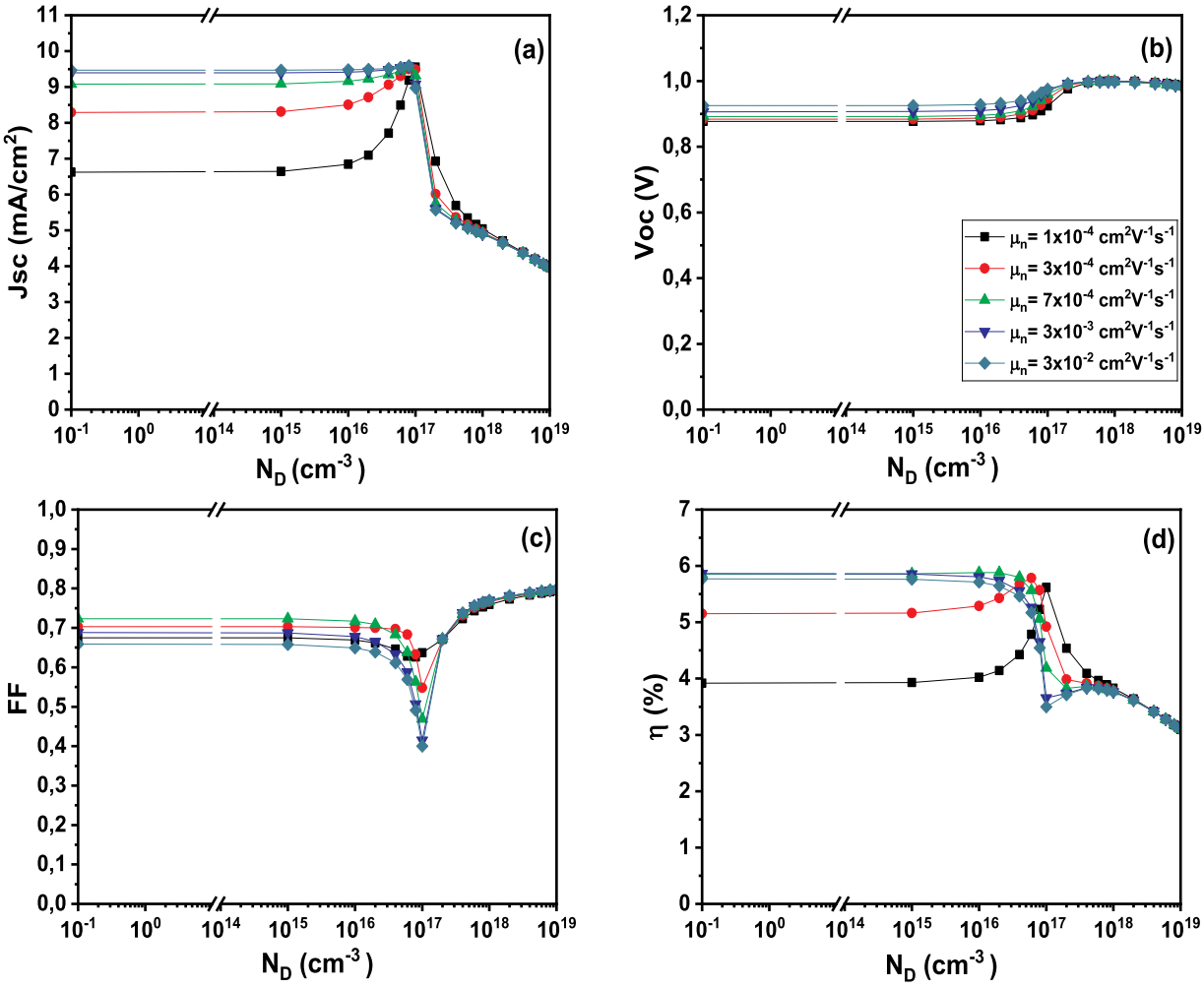

Fig. 7. The effect of N-type doping concentration N_D on the performances of P3HT: $IC_{60}BA$ based solar cell for different electron mobilities.

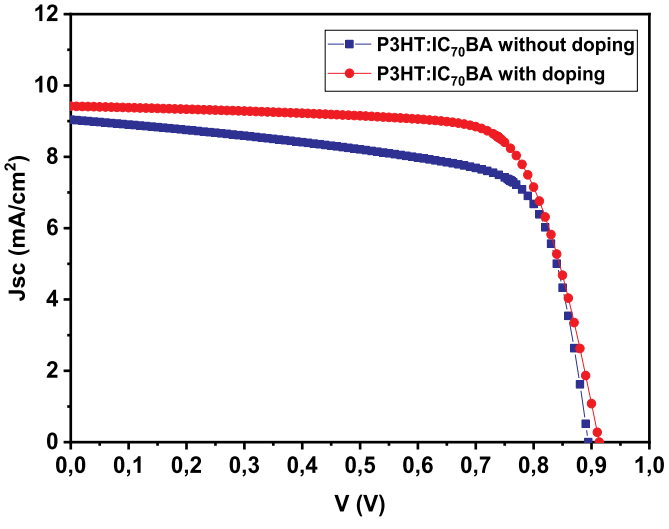

Fig. 8. J–V characteristics of the OPV solar cell based on P3HT: $IC_{70}BA$; without doping (blue color) and with doping (red color).

after doping (red color) where the variation of carriers charge mobility of electrons and holes has been taken into account by reference to the findings in previous sections for P3HT: $IC_{60}BA$. As clearly shown in Figure 8, the addition of a concentration of P-type dopant ($N_A = 1 \times 10^{17}$ cm^{-3}) exhibited a positive effect on J–V characteristics, as well as on the shunt and series resistances, and consequently on the performances of the organic solar cell based on P3HT: $IC_{70}BA$. Indeed, the performances are noticeably improved, which pass from $J_{sc} = 9.04\,mA/cm^2$, $V_{oc} = 0.89$ V, FF = 0.69 and $\eta = 5.57\%$ to $J_{sc} = 9.42\,mA/cm^2$, $V_{oc} = 0.91$ V, FF = 0.73 and $\eta = 6.32\%$, respectively, representing an enhancement rate in the efficiency of about 13.4% (Tab. 3). Moreover, this efficiency value of the OPV based on P3HT: $IC_{70}BA$ doped by P-type dopant remains more interested compared to that of P3HT: $IC_{60}BA$.

4 Conclusion

In summary, the effect of doping concentrations (P-type and N-type) of the active layer on the performances of an

Table 3. Optimal performance of the OPV solar cell based on P-doped P3HT: $IC_{70}BA$.

	Without doping		With doping
	Experiment [48]	Simulation	Simulation
N_A (cm^{-3})	–	4×10^{16}	1×10^{17}
η (%)	5.46	5.57	6.32
FF	0.70	0.69	0.73
J_{sc} (mA/cm^2)	9.70	9.04	9.42
V_{oc} (V)	0.84	0.89	0.91

organic solar cell based on P3HT: $IC_{60}BA$ has been investigated through the application of an effective medium model (EMM) by using AMPS-1D software. Moreover, the combination of N-type doping concentration and electrons mobility effects was proposed as an original approach. As result, we have discovered that the doping does not always improve the performance of the device but, this depends on the type of dopant as well as its value. In addition, we noticed that the P-type doping has more potential effect than N-type one for the performances improvement of the P3HT: $IC_{60}BA$ based OSC, and especially when the values of carriers mobility are enough low. Thus, this improvement was noticed when the ratio of electrons and holes mobility μ_n/μ_p is shifted to 1. Furthermore, a high *eff*iciency of 5.88% was achieved for particular values of $N_A = 1 \times 10^{17} cm^{-3}$, $N_D = 2 \times 10^{16}$ cm^{-3}, $\mu_p = 3 \times 10^{-4}$ cm^2 V^{-1} s^{-1} and $\mu_n = 7 \times 10^{-4}$ cm^2 V^{-1} s^{-1}. These simulation results for P3HT: $IC_{60}BA$ device, were validated by those experimentally ones reported in literature. In addition, the application of P-type doping has been done also for the first time on another BHJ OSCs based on P3HT: $IC_{70}BA$. Indeed, these results remain enough encouraged to dope and realize this type of device for use in low power applications [50].

Nomenclature

ε_r	Relative permittivity
ε	Permittivity
μ_n	Electron mobility
μ_p	Hole mobility
N_D	Concentration of donor-dopant
N_A	Concentration of acceptor-dopant
E_g^{eff}	Effective band gap
N_C	Effective density of states in the conduction band at temperature T
N_V	Effective density of states in the valence band at temperature T
χ	Electron affinity
Ψ	Electrostatic potential
n	Free electron density
	p Free hole density
J_n	Current density of electron
J_p	Current density of hole
n_t	Trapped electron density
p_t	Trapped hole density
N_D^+	Ionized donor-like doping
N_A^-	Ionized acceptor-like doping
T	Temperature
q	Magnitude of the charge of an electron
$R(x)$	Net recombination rate
$G(x)$	Electron-hole pair generation rate

The authors would like to thank Professor S. Fonash of the Pennsylvania State University for providing the AMPS-1D program used in the simulations. Thus, the acknowledgments are destined to the National Center for Scientific and Technical Research (CNRST) for supporting our study in Excellence Grant Program 2017.

Author contribution statement

Meriem Erray: was mainly contributed to the preparation of the paper as well as references and the curves illustrated in the manuscript. Moreover, she contributed to the numerical simulations investigated on ITO/PEDOT: PSS/P3HT: $IC_{60}BA$/Ca/Al structure with Analysis of Microelectronic and Photonic Structures the simulation one dimension software (AMPS-1D). In addition, she contributed to the results discussion and interpretation, and also to the responses to reviewers comment.
Aumeur El Amrani: was contributed to the paper as the supervisor of the investigated research work. Thus, he contributed to the correction of the paper as well as to the results discussion and interpretation, and also to the responses to reviewers comment.
Mounir Hanine: was contributed to the paper as the co-supervisor of the investigated research work. He also contributed to the organization of the manuscript.
Mohamed El Amraoui: was contributed to the results discussion and interpretation and references checking.
Lahcen Bejjit: was contributed to the results discussion and the revision and organization of the manuscript.

References

1. J.-H. Kim, S.A. Shin, Macromolecules **47**, 1351 (2014)
2. T. Adhikari, J.-M. Nunzi, O. Lebel, Org. Electron. **49**, 382 (2017)
3. S. Wang, P. Yang, K. Chang, W. Lv, B. Mi, J. Song, X. Zhao, H. Gao, Org. Electron. **74**, 269 (2019)

4. F. Hakim, Md.K. Alam, Sol. Energy **191**, 300 (2019)
5. N.T. Ho, H.N. Tien, S.-J. Jang, V. Senthilkumar, Y.CH. Park, S. Cho, Y.S. Kim, Sci. Rep. **6**, 30327 (2016)
6. Z. Jiang, B. Gholamkhass, P. Servati, J. Mater. Res. **34**, 2407 (2019)
7. J. Khanam, S. Foo, Polymers **11**, 383 (2019)
8. M. Erray, M. Hanine, E.-M. Boufounas, A. El Amrani, Eur. Phys. J. Appl. Phys. **82**, 30201 (2018)
9. S. Lu, D. Ouyang, W.C.H. Choy, Sci. China Chem. **60**, 460 (2017)
10. Y.-Y. Yu, C. Tseng, W.-C. Chien, C.-P. Chen, Org. Electron. **69**, 20 (2019)
11. T. Adhikari, P. Solanke, D. Pathak, T. Wagner, F. Bure, T. Reed, J.-M. Nunzi, Opt. Mater. **69**, 312 (2017)
12. F. Wei, L. Yao, F. Lan, G. Li, L. Liu, Beilstein J. Nanotechnol. **8**, 123 (2017)
13. T. Adhikari, Z. Ghoshouni Rahami, J.-M. Nunzi, O. Lebel, Org. Electron. **34**, 146 (2016)
14. B. Kadem, W. Cranton, A. Hassan, Org. Electron. **24**, 73 (2015)
15. O. Oklobia, T.S. Shafai, Sol. Energy Mater. Sol. Cells **122**, 158 (2014)
16. G. Li, V. Shrotriya, Y. Yao, Y. Yang, J. Appl. Phys. **98**, 043704 (2005)
17. J. Müllerová, M. Kaiser, V. Nádaždy, P. Šiffalovič, E. Majková, Sol. Energy **134**, 294 (2016)
18. W. Aloui, T. Adhikari, J.-M. Nunzi, A. Bouazizi, K. Khirouni, Mater. Sci. Semicond. Process. **39**, 575 (2015)
19. Y. He, H.-Y. Chen, J. Hou, Y. Li, J. Am. Chem. Soc. **132**, 1377 (2010)
20. G. Zhao, Y. He, Y. Li, Adv. Mater. **22**, 4355 (2010)
21. Z. Tan, D. Qian, W. Zhang, L. Li, Y. Ding, Q. Xu, F. Wang, Y. Li, J. Mater. Chem. A **1**, 657 (2013)
22. S. Gärtner, M. Christmann, S. Sankaran, H. Röhm, E.-M. Prinz, F. Penth, A. Pütz, A. Türeli, B. Penth, B. Baumstümmler, A. Colsmann, Adv. Mater. **26**, 6653 (2014)
23. E.F. Oliveira, L.C. Silva, F.C. Lavarda, Struct. Chem. **28**, 1133 (2017)
24. T. Adhikari, S.R. Bobbara, J.-M. Nunzi, O. Lebel, Org. Electron. **53**, 74 (2018)
25. J. Yuan, J. Gu, G. Shi, J. Sun, H.-Q. Wang, W. Ma, Sci. Rep. **6**, 26459 (2016)
26. X. Che, Y. Li, Y. Qu, S.R. Forrest, Nat. Energy **3**, 422 (2018)
27. J.Y. Kim, K. Lee, N.E. Coates, D. Moses, T.-Q. Nguyen, M. Dante, A.J. Heeger, Science **317**, 222 (2007)
28. C. Liu, Z. Li, Z. Zhang, X. Zhang, L. Shen, W. Guo, L. Zhang, Y. Long, S. Ruan, Phys. Chem. Chem. Phys. **19**, 245 (2017)
29. X. Guo, C. Cui, M. Zhang, L. Huo, Y. Huang, J. Hou, Y. Li, Energy Environ. Sci. **5**, 7943 (2012)
30. K. Walzer, B. Maennig, M. Pfeiffer, K. Leo, Chem. Rev. **107**, 1233 (2007)
31. A. Barbot, Thesis, University of Limoges, France (2014)
32. X. Lin, Ph.D. thesis, Princeton University, United States – New Jersey (2018)
33. Y. Xu, J. Yuan, J. Sun, Y. Zhang, X. Ling, H. Wu, G. Zhang, J. Chen, Y. Wang, W. Ma, ACS Appl. Mater. Interfaces **10**, 2776 (2018)
34. J. Euvrard, A. Revaux, A. Cantarano, S. Jacob, A. Kahn, D. Vuillaume, Org. Electron. **54**, 64 (2018)
35. H. Akamatu, H. Inokuchi, Y. Matsunaga, Nature **173**, 168 (1954)
36. I. Tchouar (née Malti), thesis, University Abou-BekrBelkaïd, Tlemcen, Algérie (2015)
37. D.T. Scholes, Ph.D. thesis, Ann Arbor, United States (2018)
38. D.R. Kearns, G. Tollin, M. Calvin, J. Chem. Phys. **32**, 1020 (1960)
39. M. Erray, M. Hanine, A. El Amrani, Optik **202**, 163543 (2020)
40. M.G. Ramsey, D. Steinmüller, F.P. Netzer, Phys. Rev. B **42**, 5902 (1990)
41. Y. Lin, Y. Firdaus, M.I. Nugraha, F. Liu, S. Karuthedath, A.-H. Emwas, W. Zhang, A. Seitkhan, M. Neophytou, H. Faber, E. Yengel, I. McCulloch, L. Tsetseris, F. Laquai, T. Anthopoulos, Adv. Sci. **7**, 1903419 (2020)
42. M.T. Fontana, Ph.D. thesis, Ann Arbor, United States (2018)
43. C. Herold, R. Yazami, D. Billaud, Polym. Solide **309**, 1365 (1989)
44. I.P. Kozlov, V.B. Odzhaev, I.A. Karpovich, V.N. Popok, D.V. Sviridov, J. Appl. Spectrosc. **65**, 390 (1998)
45. B.M. Omer, Phys. Status. Solidi A **213**, 2518 (2016)
46. B.M. Omer, A. Khogali, A. Pivrikas, in *Proceedings Photovoltaic Specialists Conference (PVSC), 2011 37th IEEE*, 000734 (2011)
47. A.B. Walker, A. Kambili, S.J. Martin, J. Phys.: Condens. Matter. **14**, 9825 (2002)
48. Y. He, G. Zhao, B. Peng, Y. Li, Adv. Funct. Mater. **20**, 3383 (2010)
49. Y. Zhang, H. Zhou, J. Seifter, L. Ying, A. Mikhailovsky, A.J. Heeger, G. Bazan, T.-Q. Nguyen, Adv. Mater. **25**, 7038 (2013)
50. A. El Amrani, M. El Amraoui, A. El Abbassi, C. Messaoudi, Superlattices. Microstruct. **75**, 39 (2014)

Cite this article as: Meriem Erray, Aumeur El Amrani, Mounir Hanine, Mohamed El Amraoui, Lahcen Bejjit, Improving photovoltaic performance of P3HT: $IC_{60}BA$ based organic solar cell: N-type doping *eff*ect, Eur. Phys. J. Appl. Phys. **97**, 23 (2022)